PAPER

# Time-resolved electron energy distribution functions at the substrate during a HiPIMS discharge with cathode voltage reversal

To cite this article: Wolfgang Huber *et al* 2022 *Plasma Sources Sci. Technol.* **31** 065001

View the article online for updates and enhancements.

You may also like

- Diagnosing asymmetric bipolar HiPIMS discharges using laser Thomson scattering
Marcus A Law, Francis Lockwood Estrin, Mark D Bowden et al.
- New procedure to estimate plasma parameters through the q-Weibull distribution by using a Langmuir probe in a cold plasma
F J Gonzalez, J I Gonzalez, S Soler et al.
- The impact of Langmuir probe geometries on electron current collection and the integral relation for obtaining electron energy distribution functions
Ahmed El Saghir and Steven Shannon

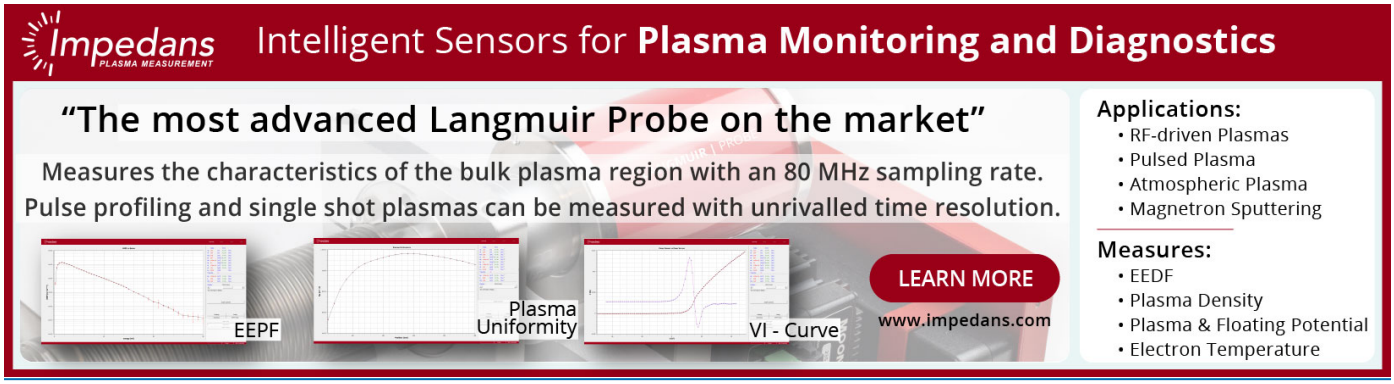


This content was downloaded from IP address 192.17.21.160 on 21/06/2022 at 17:40

IOP Publishing Plasma Sources Science and Technology
Plasma Sources Sci. Technol. **31** (2022) 065001 (10pp) https://doi.org/10.1088/1361-6595/ac6d0a

# Time-resolved electron energy distribution functions at the substrate during a HiPIMS discharge with cathode voltage reversal

**Wolfgang Huber[1], Thomas Houlahan[2], Zachary Jeckell[1], David Barlaz[1], Ian Haehnlein[2], Brian Jurczyk[2] and David N Ruzic[1,*]**

[1] Department of Nuclear, Radiological, and Plasma Engineering, University of Illinois at Urbana-Champaign, Urbana, IL, United States of America
[2] Starfire Industries, Champaign, IL 61820, United States of America

E-mail: druzic@illinois.edu

Received 6 April 2022
Accepted for publication 5 May 2022
Published 6 June 2022

**Abstract**

The time-dependent plasma properties of a high-power impulse magnetron sputtering plasma are investigated which include a positive 'kick' pulse on the sputtering target 2 $\mu$s after the main negative pulse, this reversing the voltage on the cathode. At a substrate 15 cm distant from the magnetron, the time-dependent electron energy distribution function (EEDF), plasma potential, potential commute time and plasma diffusion properties are measured using a single Langmuir probe. Results show that the positive pulse on the target expels plasma and raises the plasma potential across the chamber on the order of 1 to 2 $\mu$s, which is the time scale of the electron diffusion. The EEDF at the substrate fits a Druyvesteyn distribution during the main negative pulse rising slightly in average energy over time. The distribution is still Druyvesteyn and at the very start of the positive pulse, but then loses the higher energy electrons and drops in average electron energy as the positive pulse progresses. A Boltzmann equation solver, BOLSIG+, was used to predict the EEDF at the substrate during the positive pulse and it agrees best with the measurements assuming a value of 0.2 Td for the *E*/*N* (electric field/gas number density).

Keywords: HiPIMS, EEDF, Langmuir probe, plasma, time resolved

(Some figures may appear in colour only in the online journal)

## 1. Introduction

High-power impulse magnetron sputtering (HiPIMS) is an established method for magnetron sputtering using a negative standard magnetron pulse (main pulse) to strike and sustain a high density plasma while keeping the time average power low. HiPIMS is often supplemented with a positive voltage pulse (kick pulse) applied to the cathode following the main pulse after a short transistor switching delay time. HiPIMS with the cathode-voltage reversal is a growing research interest for thin film deposition because of its ability to tune ion energies to a desired value referred to as the applied positive voltage [1]. A typical HiPIMS pulse is depicted below in figure 1, with the positive pulse reversal and afterglow regions added after the traditional HiPIMS main pulse. This waveform was captured as part of our experimental procedure, and is representative of the HiPIMS plasma used in our experiments.

HiPIMS provides advantages over chemical vapor deposition and DC magnetron sputtering (dcMS) in control over conformality, film stress, and grain structure that have been used to deposit high quality copper, niobium, and titanium nitride as well as other materials [1–4]. Many of those advantages come from applying a positive voltage pulse—often referred to as a positive voltage reversal or Positive Kick$^{TM}$—to the

* Author to whom any correspondence should be addressed.

 © 2022 IOP Publishing Ltd Printed in the UK

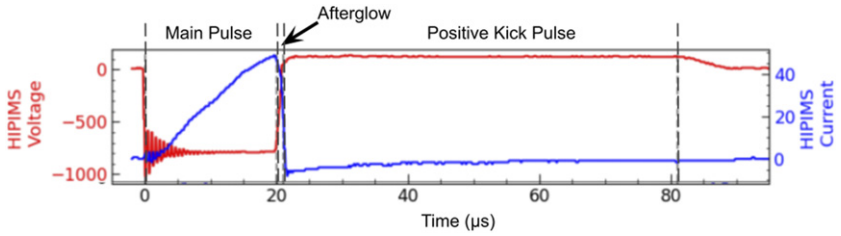


**Figure 1.** A diagram of a HiPIMS pulse and its corresponding parts and terminology. Pulse voltage in shown in red, and current in blue. The afterglow region is between the main pulse and positive pulse and has a length of 2 $\mu$s.

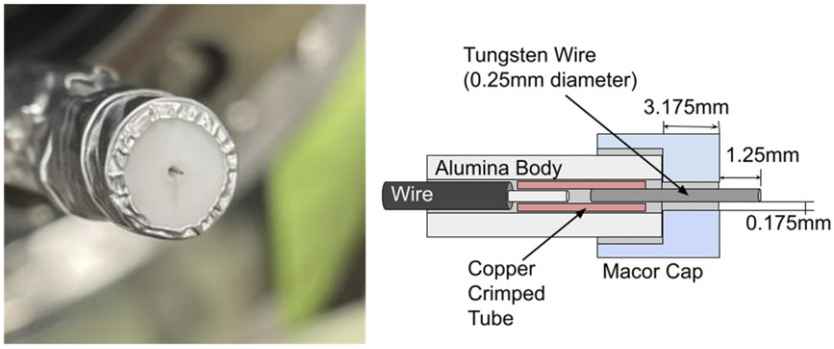


**Figure 2.** Langmuir probe assembly and dimensions are depicted here. In the left image is the Langmuir probe with a tungsten probe tip length of 1.2 mm and diameter of 0.25 mm. The Macor$^{TM}$ body has a diameter of 8.128 mm and is shielded with aluminum ultra high vacuum foil and braided stainless steel mesh along the cable.

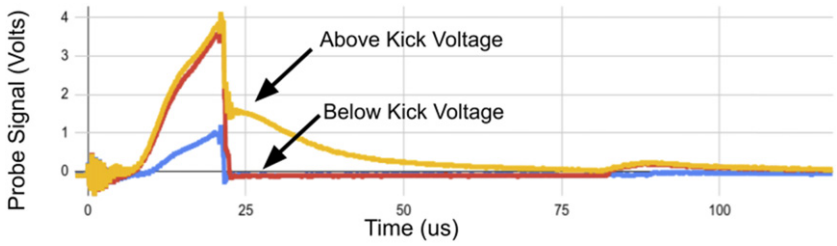


**Figure 3.** Probe response to different voltages shown. Yellow is 130 V, red is 110 V, and blue is 30 V. Kick voltage is 120 V for the corresponding pulse and the main pulse width is 20 $\mu$s and kick pulse width is 50 $\mu$s. The probe current in the kick is shown to drastically change above the kick voltage.

magnetron target within a few microseconds of the termination of the negative 'main' pulse [5]. Higher positive voltages have been correlated to higher film density, hardness, and compressive stress [1, 2]. Using a positive pulse following the main pulse has already been shown to allow for control of the film tensile stress in copper depositions while also increasing metal ion flux to the substrate, which significantly increases the deposition rate using a standard magnet pack [6]. Altering the magnet pack has been shown to increase the deposition rate and ion fraction even further, especially if the positive pulse is added as with certain magnet pack designs [7].

To fully understand these phenomena and expand its application in industry, a better understanding of how the HiPIMS pulse settings and chamber geometry affect the plasma and the consequent film properties is required. Characterizing the electron energy distribution function (EEDF) can reveal key insights into diffusion, conformality, and reaction rates affecting the plasma chemistry, which is of great interest for reactive sputtering applications. Understanding the temporal evolution of the distribution function and key parameters such as the electron density and plasma potential can allow for precise control over the populations of reactive intermediates such as those produced from nitrogen or oxygen. The temporal evolution of the plasma potential, floating potential, and electron density have been demonstrated both for traditional [8–14] and for bipolar HiPIMS [15–17], however the EEDF, especially for systems with short afterglow times (on the order of 2 $\mu$s) have yet to be analyzed for bipolar HiPIMS. Shorter afterglow times between the main pulse and the kick pulse are of particular interest because it allows less time for the dense plasma near the target and within the magnetic trap to diffuse toward the walls, and is instead influenced by the positive voltage pulse. Knowledge of time at which the peak plasma density is reached can allow for the creation of deposition processes that best leverage the advantages afforded by the positive voltage pulse. Additionally, investigation into the time-dependence of the

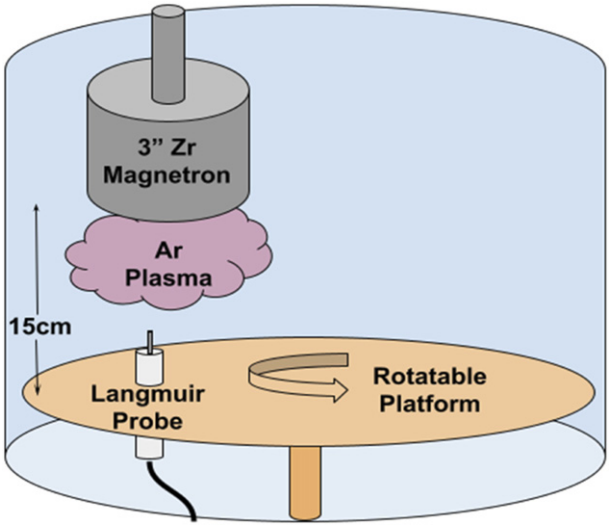


**Figure 4.** The chamber configuration and geometry of the argon plasma sputtering zirconium onto a large grounded surface with the Langmuir probe protruding up from the ground platform which would hold a substrate. The probe can be rotated out of the way to avoid deposition when not in use.

EEDF and other plasma parameters. This research sheds light into: the transport method of the plasma potential; the bulk plasma electron and ion energies; the sheath's time dependent effect during the positive voltage pulse; and finally the effect of the positive pulse on the incident electron and ion energies at the substrate. Characterizing these parameters throughout the HiPIMS waveform at the substrate location with an afterglow duration of 2 $\mu$s is demonstrated in this work.

## 2. Experimental details

### 2.1. Experiment setup

The time-resolved EEDF measurements were performed using a single Langmuir probe. Over the course of a single HiPIMS pulse the probe was held at a constant bias and the current was measured as a function of time. This measurement was repeated over a series of consecutive pulses to verify consistent pulse-to-pulse stability in the waveforms. The probe bias voltage was then stepped and the procedure was repeated, following the technique first demonstrated in references [18, 19] for a 13.56 MHz RF plasma and more recently in references [13, 14] for HiPIMS plasmas. The Langmuir probe itself was built in-house. As shown in figure 2, it had a tungsten tip with a diameter of 0.25 mm and a length of 1.2 mm. The body was manufactured from alumina and Macor™ and covered in grounded shielding. The probe was installed perpendicular to the plane of the substrate and had a replaceable cap to prevent significant buildup of deposited metal in and on the probe. The probe was mounted on a rotatable substrate holder that allowed it to be moved away from the magnetron. This was done to minimize deposition on the probe tip when it was not in use.

The probe was connected to a custom control and measurement circuit capable of applying bias voltages in the range of −150 V to +400 V and measuring probe currents through a 1 Ω current sense resistor. Since the probe routinely struck a local plasma above +300 V, it was limited to +250 V and operated with a step size of approximately 0.75 V. An example set of probe-current waveforms, exhibiting a temporal resolution on the order of ∼0.1 $\mu$s, is shown in figure 3 for three selected bias voltages. These waveforms were collected from our experimental results and correspond with the waveform shown in figure 1.

The EEDF measurement technique was performed in a high vacuum chamber, depicted in figure 4, with a chamber base pressure of $4 \times 10^{-6}$ Torr. The working gas used was argon. To generate the HiPIMS discharge a Starfire Industries IMPULSE® 20–20 with Positive Kick™ was used to drive a 3″ TORUS® magnetron with a corresponding zirconium target. The IMPULSE® 20–20 was powered by two SL-series, 2.6 kW, Magna-Power DC supplies. The substrate holder was rotatable, height-adjustable, and could be modified to have a large or small ground plane.

To limit the power drawn from the measurement circuit, the impulse unit was limited to frequencies less than 2 kHz and the main pulse width less than 50 $\mu$s. Additionally, only stable plasmas having little shot-to-shot variation were used in these measurements. We additionally chose a 20 $\mu$s main pulse width since this was the time required for the main pulse plasma to rarify given the other process condition limitations. The kick pulse was chosen to extended for 60 $\mu$s to allow for analysis of short and long kick effects on the plasma. The operating pressure range was 5–20 mTorr. All of these discharges were also allowed to settle and warm up to minimize drift as the measurements were taken over a 15 min time span. This typical HiPIMS waveform is shown in figure 1. Lastly, a cleaning step was run following every vent cycle, immediately after pumping the chamber down from atmospheric pressure. This cleaning step was composed of a 8 KHz squarewave-like HiPIMS pulse with an amplitude of 400 V in a mix of 5% oxygen and 95% argon plasma. These pulse characteristics result in etching the chamber walls and sputtering surface contaminants off the magnetron.

### 2.2. Data processing

To process the data, established methods from references [20, 23], and [22] were used to extract plasma parameters. Extracting a time-dependent EEDF from the recorded data required combining the recorded $I(t)$ waveforms taken over a discrete set of bias voltages into a single dataset. First, for each waveform, the actual probe voltage was computed by subtracting the voltage across the current sensing resistor from the measured DC bias voltage. Both the measured $I(t)$ and the computed $V(t)$ waveforms were then combined into a single dataset, where each point in the set is specified by a $(t, I, V)$ ordered triplet. The surface described by these data was then interpolated over an evenly spaced set of times and probe voltages ($t$ and $V$, respectively) to enable the straightforward extraction of $I$–$V$ traces over a discrete set of times. This interpolated surface is shown in figure 5. This interpolation was done supplementary to the steps performed in reference [22] and is necessary due to the uneven spacing that occurs in the bias voltage axis. This is due not only to the time-dependent

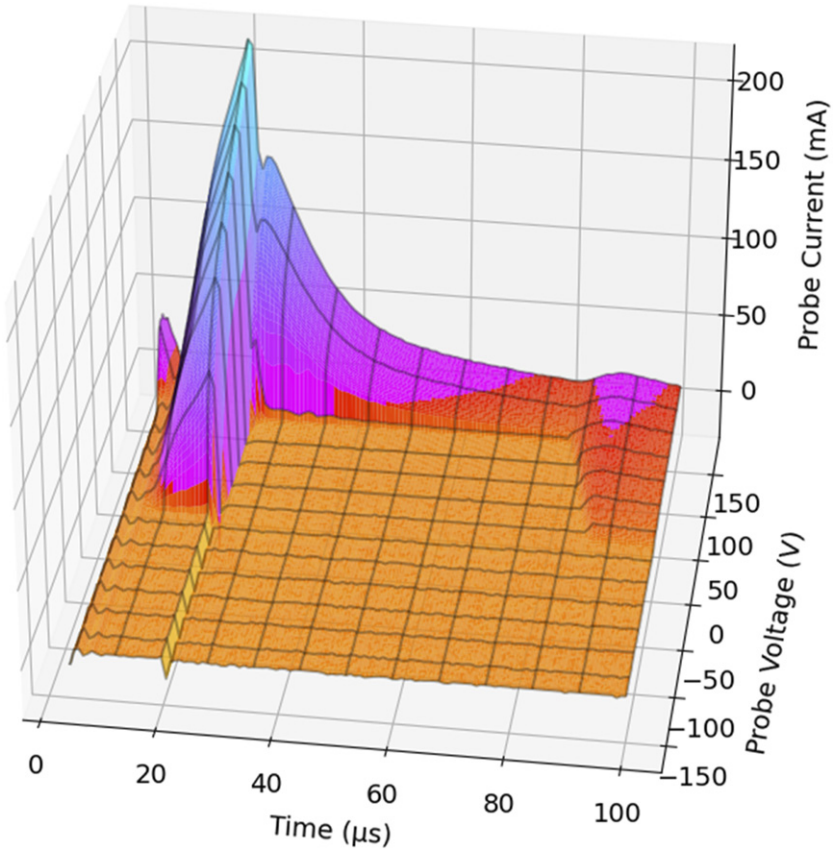


**Figure 5.** A uniform surface of probe voltage, current and time from a surface of stacked probe current vs time at different voltages. This is the measured Langmuir probe data for the waveform shown in figure 1.

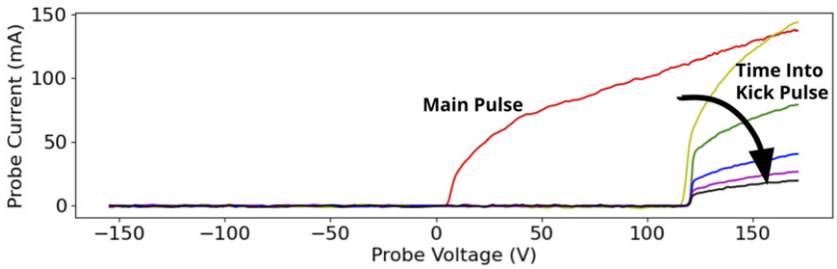


**Figure 6.** In blue is a current–voltage trace at 14 $\mu$s (main pulse). Orange, green, red, purple, and brown are in the kick pulse at 26 $\mu$s, 38 $\mu$s, 50 $\mu$s, 62 $\mu$s, and 75 $\mu$s respectively. The floating and plasma potential increase from ∼10 V to 120 V when the 120 V kick voltage is applied. The current is positive in the ion saturation regions.

variation in the probe voltage resulting from the voltage drop across the current sense resistor, but also to the deliberate, intentional variation in voltage steps to speed up the collection processes over regions where the probe current does not change very much (i.e. for $V \ll 0$). Figure 5 shows the scale of electron current to ion current for our measurements and gives a good approximation for how the total plasma density changes by looking at the electron saturation region.

The interpolated data is then partitioned into subsets having identical time-values, where each subset is a distinct $I$–$V$ curve for a given time in the HiPIMS pulse and the dataset as a whole is the full set of $I$–$V$ curves for a discrete set of times spanning the entire HiPIMS pulse. Figure 6 shows a set of $I$–$V$ curves extracted in this way for a selected set of times spanning both the main and positive kick pulses. References [20, 21] provide a detailed description on the extraction of information about the plasma from $I$–$V$ curves. In an $I$–$V$ slope, the plasma potential is located at the minimum extrema of the first derivative and the EEDF is related to the second derivative.

While first and second derivatives of the probe current with respect to the probe voltage are required for determining the EEDF, the inherent sensitivity of numerical differentiation to noise is such that direct, numerical differentiation is not

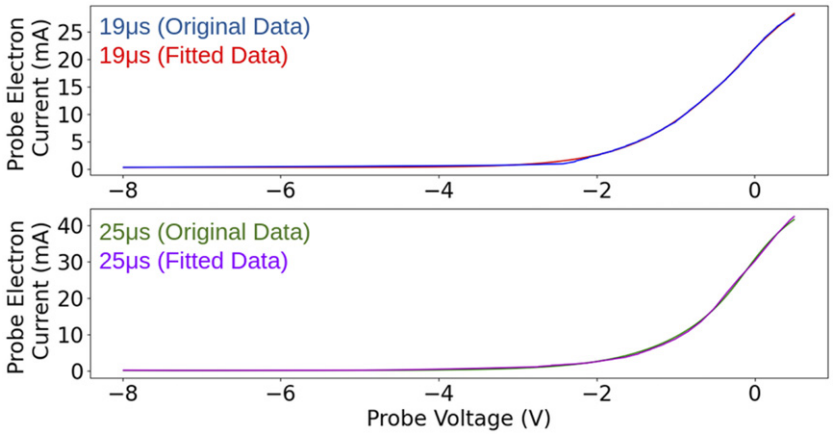


**Figure 7.** The fits using a set of generic negative concavity and slope functions plotted against the original interpolated data for both slices occurring in the main pulse (19 $\mu$s) and in the kick pulse (25 $\mu$s).

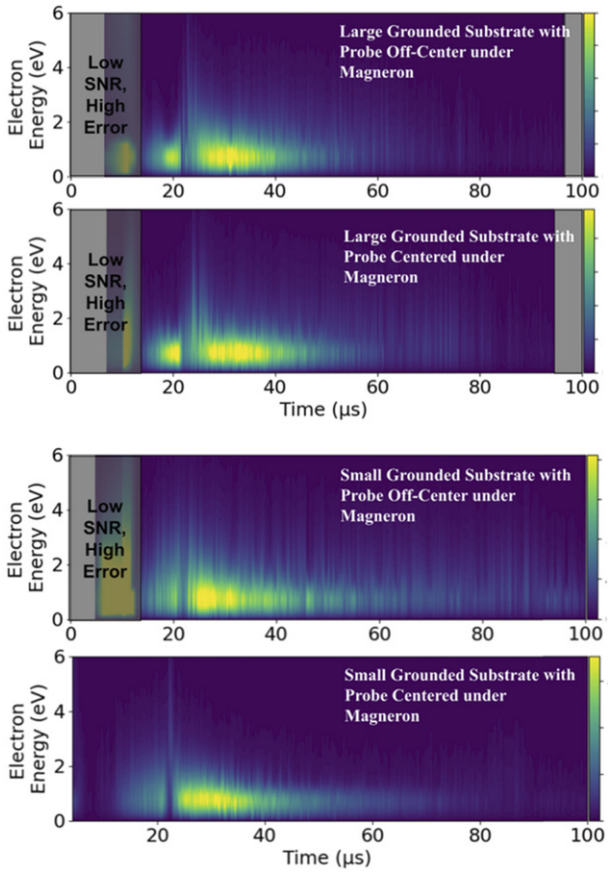


**Figure 8.** A false color normalized EEDF is depicted with the color corresponding to the number of electrons at that energy. The far right-hand side of the figure shows the linear color scale magnitude. The data for the first three cases from 0 to 12 microseconds has low signal to noise. These results are for the waveform shown in figure 1, but with a positive voltage reversal of 100 V. Note the apparent lack of low energy electrons at 22 $\mu$s independent of how the substrate was grounded.

feasible. Following Ruzic [20], least-squares fitting using polynomial, generic negative sloped, and generic negative concavity functions were applied to the $I$–$V$ traces and used in place of the interpolated $I$–$V$ trace data in computing the first and second derivatives.

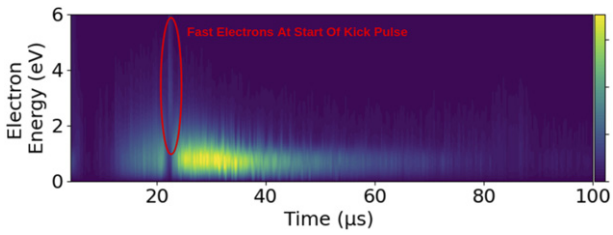


**Figure 9.** An example EEDF that shows very fast electrons drawn to the target, thereby raising the plasma potential and commuting it to the substrate at the start of the positive pulse. These fast electrons are circled in red.

The first step in extracting EEDFs from the $I$–$V$ traces is to determine the plasma potential, as computing the EEDF requires this information. The plasma potential is defined as the point in the $I$–$V$ trace where the slope of the electron current is at a maximum. Using methods from Ruzic in reference [20] we find the plasma potential and approximate the ion current according to equation (1) below. The ion current approximation as according to reference [20]

$$I_{\mathrm{i}} = \frac{1}{4} \cdot q n_{\mathrm{e}} \sqrt{\frac{8kT_{\mathrm{e}}}{\pi m_{\mathrm{i}}}} \cdot A_{\mathrm{probe}} \cdot \sqrt{\frac{q(V_{\mathrm{p}} - V)}{kT_{\mathrm{e}}}}. \qquad (1)$$

With the ion saturation current known, a solution of the ion current as a function of the probe voltage is found. This expression for the ion current is then subtracted from the total current to yield the electron current.

With knowledge of the plasma potential and electron current, it is then possible to calculate the EEDF as outlined in references [20, 21]. The first step is to subtract the plasma potential from the probe voltage measured. This is to remove the energy measured as given to the plasma by the sheath to measure the EEDF as it would be in the bulk plasma. Next, another fit on the electron probe current is applied. This fit will be used to calculate second derivatives and therefore will be sensitive to noise. To reduce error, analysis was limited to voltages between the plasma potential and data 12 V below it. These fits can be seen in figure 7 and are shown to have a low standard deviation from the original data.

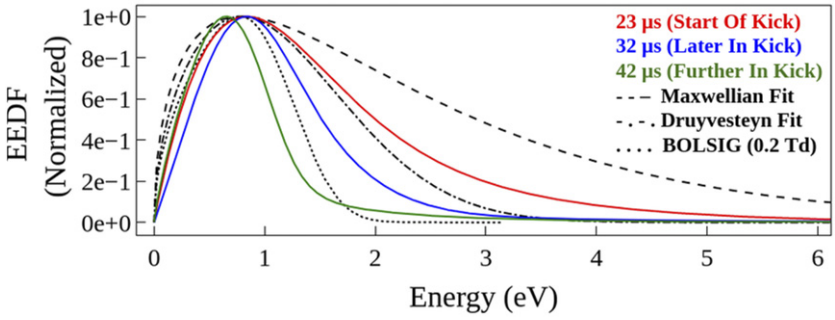


**Figure 10.** The electron energy distribution at 23, 32, and 42 $\mu$s, which are points in time when the plasma potential has reached a constant value in the kick pulse at the substrate. At this point the entire 100 V potential is across the sheath at the substrate. The BOLSIG+ [32] plot (dotted line) is calculated from a Boltzmann solver and the Biagi v7.1 argon data set [33] from LCAT [34] using 0.2 Td as the *E*/*N* value. The value of 0.2 Td corresponds to a less than one half volt potential drop between the target and the probe location.

To fit to the $I$–$V$ trace the least square error between the $I$–$V$ trace and the function described in equation (2) was minimized. The minimized function that fits to the $I$–$V$ trace was chosen because it has a continuous negative concavity and negative slope. This fit is representative of a real EEDF with no negative density and increasing electron current that occurs with increasing probe voltage. A single term has the form of a generalized EEDF [23]. For each term $E_n$ and $A_n$ were left floating in addition to the offset variable $C_0$ and the exponential rise factor $C_1$ for the minimization function to solve. In fitting, six terms proved sufficient as higher orders had negligible contributions. An example of fits compared to original data is shown in figure 7 for times in the main and kick pulse. There it is demonstrated that the fit and original data match well. The function to which $I$–$V$ trace is fit

$$F(E) = C_0 + \iint \sum_{1}^{5} A_n \cdot E^{C_1} \cdot e^{-\left(\frac{E}{E_n}\right)^n} \mathrm{d}V^2. \qquad (2)$$

The EEDF was obtained using a numerical second derivative of the fitted $I$–$V$ trace, the probe voltage, and following the relation in equation (3) [20, 21]. The EEDF formula according to reference [20]

$$f_e = \frac{-4 \cdot 10^{-6}}{A_{\mathrm{probe}} \cdot q} \sqrt{\frac{m_e(V_p - V)}{2q}} \cdot \frac{\mathrm{d}^2 I_e(V)}{\mathrm{d}V^2}. \qquad (3)$$

$A_{\mathrm{probe}}$ is the surface area of the Langmuir probe tip, $q$ is the elementary charge and $V_p$ is the plasma potential, and $I_e$ is the electron current as a function of voltage. Using this relation, an EEDF at every single time is generated.

Applying this procedure to the full set of $I$–$V$ curves yields the time-dependent EEDF, a false color image of which can be generated. The total electron density as a function of time can be obtained by integrating the EEDF at each time-step.

## 3. Results and discussion

Results showing EEDFs at the substrate as a function of time were obtained by analyzing several settings for different HiPIMS plasmas. With this data it is possible to make several observations and conclusions about HiPIMS plasmas with a positive reversal of the cathode voltage.

### 3.1. EEDF analysis

Several chamber geometry configurations were tested with a fixed HiPIMS waveform and were processed using the aforementioned methods. These EEDFs are plotted in figure 8.

In all four panels of figure 8 an interesting feature appears at 22 $\mu$s—just after the positive kick is applied. At this time, the EEDF is observed to shift to higher energies. On the plots the 1 to 2 eV range, where the bulk of electrons usually appear, is dark blue indicating no electrons at those energies. At the same time, there is a light blue streak at higher energies. This is a visualization of fast electrons at the very start of the bipolar kick which likely are drawn toward the target thereby making the plasma positive and commute the plasma potential to the substrate as discussed further in section 3.3. Because a 100 V signal was placed on the target, these electrons could have as much as 100 eV of energy and our measurement system was unable to capture the complete EEDF. This feature was consistent across various HiPIMS settings and positioning of the ground plane to the substrate. This feature is highlighted in figure 9.

The probe is placed 15 cm from the magnetron plasma, so it is measuring the plasma which has diffused along the open field lines from the unbalanced magnetron through the neutral gas all the way to the substrate. It is often reported that the time resolved distribution functions for HiPIMS plasmas are typically found to be best fit with a bi-Maxwellian distribution for the early portions of the main pulse, with Maxwellian distributions being a better fit at later stages of the pulse [9, 10, 24, 25]. Maxwellian distributions arise when the electrons are fully thermalized, and Druyvesteyn distributions occur when elastic electron–neutral collisions dominate and when electron–electron collisions are negligible [26]. The primary observable difference between the two distributions is the significantly lower population of high energy electrons in the case of a Druyvesteyn distribution [26], which tend to occur for instances of low *E*/*N* (electric field divided by neutral gas number density) [27–29]. While a Maxwellian distribution may be expected near the target where the plasma may be completely ionized, at the substrate the plasma density is

**Table 1.** The electron temperature equivalent from the peak of the energy distributions as a function of time. The main pulse ends at 20 $\mu$s, and the kick pulse begins at 22 $\mu$s. The plasma during the kick pulse reaches a stable plasma potential value by 24 $\mu$s.

| Time ($\mu$s) | Electron temperature equivalent (eV) |
|---|---|
| 14 | $2.4 \pm 0.6$ |
| 16 | $2.5 \pm 0.6$ |
| 19 | $2.5 \pm 0.6$ |
| 24 | $2.2 \pm 0.6$ |
| 25 | $1.9 \pm 0.6$ |
| 27 | $1.8 \pm 0.5$ |
| 35 | $1.6 \pm 0.5$ |

very low compared to the neutral density. In such cases there is a low value of *E*/*N* and, as expected, a Druyvesteyn distribution best fits the EEDF recorded before the kick. As expected in figure 10, we see the measured EEDFs for different times in the main and kick pulse following these predictions. These plots demonstrate a slightly depleted Druyvesteyn distribution in the main and a very depleted Druyvesteyn distribution in the kick pulse. A Maxwellian in figure 10 overestimates the high energy electron component showing that at this distance electron–neutral collisions dominate. Several papers have also reported Druyvesteyn distributions in dcMS [27, 30], as well as in HiPIMS discharges [14, 31].

After 14 $\mu$s the magnetron plasma has entered a self-sputtering mode and is recycling most of the sputtered target ions. The plasma seen at the substrate, by contrast, is composed of fewer high-energy electrons, though the 'temperature equivalent', which for Druyvesteyn and Maxwellian distributions is defined as $1/2$ the peak temperature, shows a very modest rise (see table 1).

At the onset of the kick pulse, at 22 $\mu$s, the false-color plots in figure 8 show the presence of higher-energy electrons which have commuted the plasma potential to the substrate. At 24 $\mu$s, when the plasma potential has already shifted to the kick value, the plasma measured at the substrate once again more closely follows a Druyvesteyn distribution. There are no secondary electrons generated from the cathode driving any discharge at this point. This lack of electrons powering the plasma through additional ionizations leads to the plasma at the substrate cooling slightly over time. A look at the EEDF's in detail, most easily seen in times 25 $\mu$s and 27 $\mu$s in figure 11, show how the plasma looses even more of the higher energy components as time goes on.

Additionally we can see the depletion from a near Druyvesteyn distribution as time passes in figure 10 into an EEDF more closely resembling a model generated by BOLSIG, a Boltzmann solver.

To examine these extracted EEDFs further, an EEDF was calculated from a partial wave expansion of the Boltzmann equation using the BOLSIG+ software [21]. A reduced set of electron–argon collisions are considered [32] which include elastic scattering, their different grouped excited states, and argon ionization. These were taken from the LXCAT database [34]. The BOLSIG+ program uses a value of *E*/*N* as an input. To obtain the match shown in figure 10 a value of 0.2 Td was used for *E*/*N*. Figure 10 also compares Maxwellian and Druyvesteyn distributions with the same peak electron energy. The measured EEDF clearly has fewer high energy electrons than a Druyvesteyn distribution, however it matches well to the EEDF calculated by solving the Boltzmann equation with the collision terms for a singly-ionized Ar plasma. The value of 0.2 Td, implies that a potential drop of less than 0.5 V is present across the 15 cm distance between the probe and the target in the 20 mTorr Ar plasma. This is consistent with the data in figure 13 showing that the plasma potential at 25 $\mu$s is completely flat and at the approximate value of the cathode kick voltage.

A second BOLSIG+ calculation [32] was done using an *E*/*N* of 666 Td representing 100 V drop over 15 cm at 20 mTorr, which is the condition immediately when the kick starts. The EEDF under those conditions was a Maxwellian distribution with an electron temperature of 11.8 eV. While we were not able to measure the entire EEDF in this short time period, our measurements are consistent with a brief hot discharge existing until the positive potential applied at that cathode is manifested entirely across the sheath drop at the substrate.

### 3.2. Plasma density

An integration of the EEDF yields the total electron density ($N_e$), which is plotted as a function of time in figure 12 for a HiPIMS plasma both with and without a positive pulse voltage. It is clear that the plasma density at the substrate decreases after the end of the main pulse when there is no kick, but increases after the main pulse when a positive kick pulse is present since plasma is expelled from the magnetron.

The electron density decays completely in about 30 $\mu$s when no kick is present. With a positive voltage pulse applied to the target, the electron density did not decay as rapidly, and extended the lifetime to the full length of the positive pulse. It takes $\sim$15 $\mu$s for the plasma to decay to 50% its initial value with the positive voltage, an improvement over the $\sim$10 $\mu$s it takes for the plasma with no voltage reversal to decay to 50%. When looking at larger time scales one can see it takes $2\times$ as long for the positive-pulsed plasma to decay to 15%. These observations suggest that a sufficiently large positive voltage could sustain the plasma with the working gas and therefore perform a combination of deposition and etch with very narrow energy distribution to preferentially affect the substrate surface. Note that Hippler *et al* [16] sees the opposite effect at a similar pressure and distance from the cathode. In their work, the positive reversal voltage was 60 V as opposed to 100 V. Our hypothesis is that the larger voltage drives additional ionizations overcoming the loss to diffusion. A lower reversal voltage could result in faster dissipation as the applied voltage would merely assist in speeding up diffusion to the walls of the chamber. Future work will investigate this phenomena further.

### 3.3. Plasma potential, commute times and diffusion rates

This research was done in parallel with work on determining the time-resolved ion energy distribution function (IEDF) [35]. For both experiments the chamber pressures, magnetron

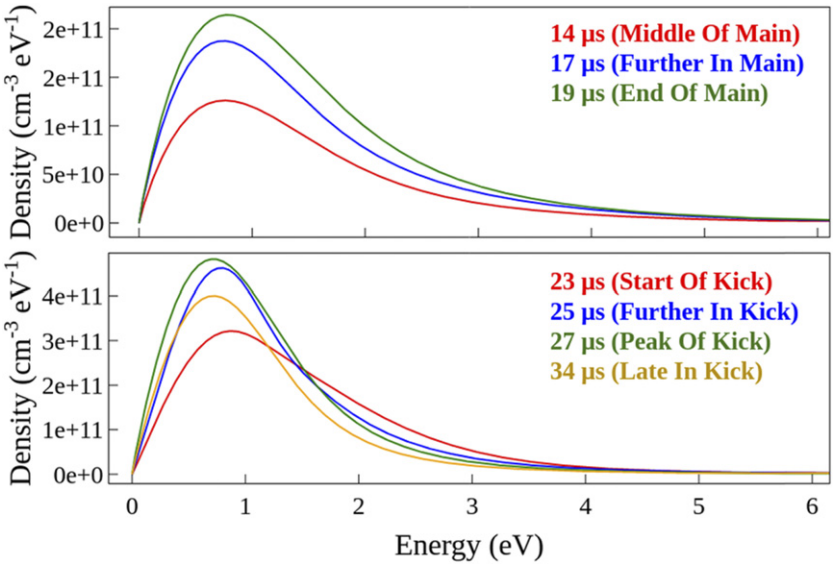


**Figure 11.** The above plots are indicative of the EEDF at 14 $\mu$s (middle of the main pulse), 17 $\mu$s (further in main pulse), 19 $\mu$s (end of main pulse), 23 $\mu$s (start of kick pulse), 25 $\mu$s (further in kick pulse), 27 $\mu$s (peak of kick pulse), 34 $\mu$s (later in kick pulse). This data set was collected at 7 mTorr of argon.

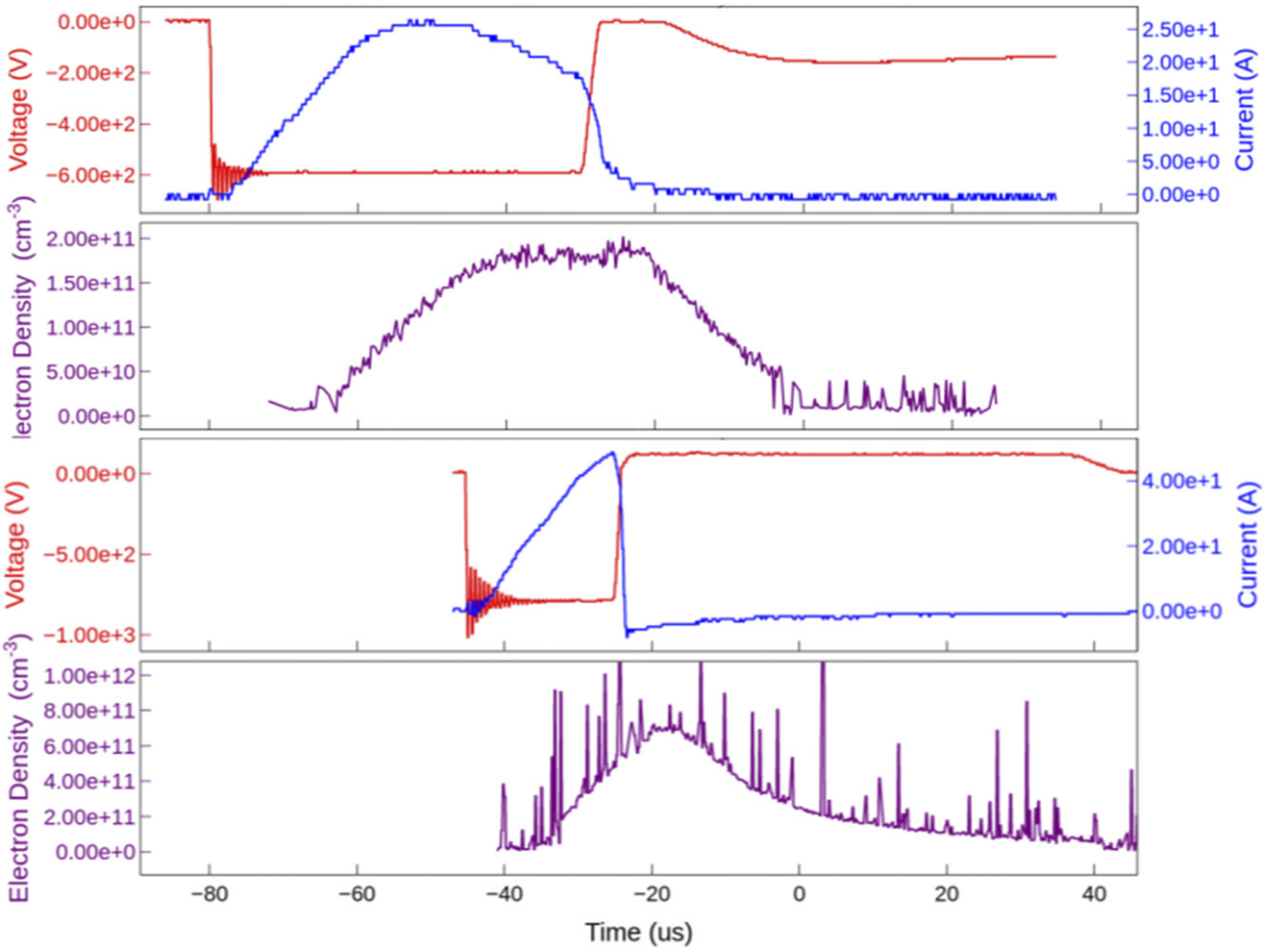


**Figure 12.** The total electron density (purple) for the corresponding HiPIMS pulse (red/blue). The top two plots are for a plasma with 50 $\mu$s main and no positive voltage reversal. The bottom plot is for the 20 $\mu$s main with a 100 V positive voltage pulse of 60 $\mu$s. Of note is the behavior after the end of the main pulse, where we see the plasma is re-energized leading to a small density rise when a positive pulse is added, and the density at the substrate actually increases. This data set was collected at 7 mTorr of argon.

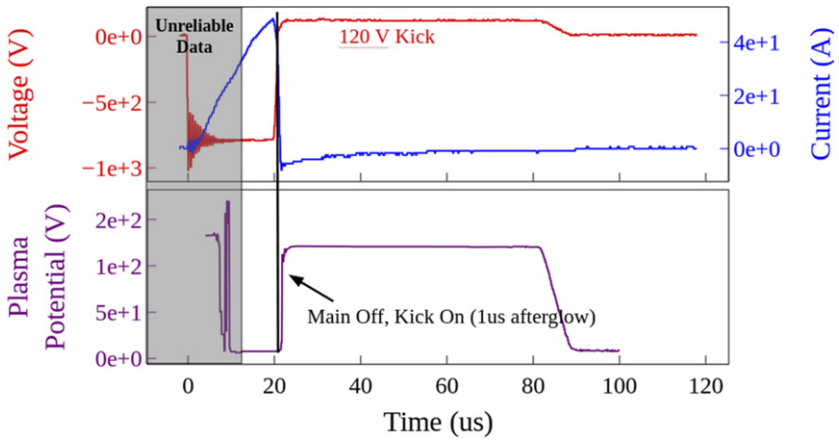


**Figure 13.** Plasma potential as a function of time at the substrate and as it corresponds to the HiPIMS pulse waveform including a positive voltage reversal on the target. In this example the plateau of the plasma potential is at the positive pulse voltage, 120 V. Plasma potential measurements before 10 $\mu$s and after 85 $\mu$s are suspect due to signal to noise limitations and range limitations of the Langmuir probe circuit. This data set was collected at 7 mTorr of argon.

target material, magnetron size, magnetron current density, and distances from magnetron were similar. The results in figure 13 show that the plasma potential commutes to the substrate between 1 and 2 $\mu$s after the kick pulse starts and completely reaches the value of the positive voltage on the substrate. The IEDF work corroborates that finding, as ion energies at the substrate were measured to rapidly shift to a value set by the applied positive pulse voltage on the same time scale [35]. In addition, by using ion data from that work, a variety of time scales can be calculated. Both experiments used a zirconium target in an argon working gas in the approximate range of 4–10 mTorr and the same main pulse and kick pulse settings. With this information it is possible to discern which mechanism, initial 'fast' electron transport or ambipolar diffusion, is responsible for commuting the plasma potential to the substrate.

The measurement shows that the plasma potential commute time was on the order of 1 to 2 $\mu$s over a distance of ∼15 cm. As an example, for a pressure of 6 mTorr, the mean free path is ∼9 mm for an electron. With the energy of an electron in the bulk plasma being close to 2 eV for both main pulse and kick pulses, it is possible to solve for a transit time $t$ where distance traveled, $\langle x^2 \rangle = 6Dt$. The diffusion constant for electrons is $D = \pi\lambda v$, where $\lambda$ is the mean free path and $v$ is the average velocity. Additionally magnetic field effects on the diffusion through the distance must be taken into account. For electron diffusion perpendicular through a magnetic field $D_e = \pi v r_{gyr}{}^2/8\lambda$, where $r_{gyr}$ is the Larmor gyro-radius of the electron. For our magnetron, the peak strength is 800 G, and this decays to 20 G at ∼3.5 cm away. 20 G is the limit where the Larmor radius is equivalent to the mean free path. This is where the electrons transition from a magnetized state to an unmagnetized state. Solving for a travel time through both these regions gives an expected travel time for an electron to diffuse through the plasma toward the target and the absence of those electrons being responsible for a rise in plasma potential going along with their motion. This travel time for electron diffusion in the plasma calculated in this manner is around 1.1 $\mu$s. The ion diffusion constant and therefore the ambipolar diffusion rate can be calculated as well. The transport time associated with the ambipolar diffusion rate is about 2.2 ms in the HiPIMS plasma. It is clear that the plasma potential is carried by the first fast electrons diffusing in the plasma to the target in response to a strong electric field, which then sets up ambipolar diffusion. The fast electrons come from the bulk plasma, originally with a low temperature, diffusing through the plasma until they reach the gradient in plasma potential. Initially this gradient is established by the magnetron now at a positive voltage, and later by the front of changing plasma conditions. At this front the electrons are accelerated by the high electric field to the target. Their initial energy at that instant approximates the change in plasma potential, typically on the order or 100 eV. This loss of electrons locally raises the plasma potential in that region, progressing the front forward. In this way the electron diffusion drives the movement of the plasma potential forward as the front of changing potential sweeps away from the magnetron. This is similar to experiments of expanding plasmas in a gaseous background, where a front of faster electrons precedes the quasineutral plasma [36]. The waterfall plot in figure 5 and the false color plots in figure 8, shows a portion of these faster electrons at times immediately after the onset of the positive kick pulse. These fast electrons would not exist in the afterglow of standard HiPIMS with no positive pulse, because standard HiPIMS units go into a high impedance mode and do not drive more plasma, as is done when the potential on the cathode is reversed.

## 4. Conclusions

A method for measuring the EEDF of a HIPIMS plasma has been applied to the case where the HIPIMS waveform has a positive voltage pulse immediately following the negative voltage pulse on the cathode. The observation of the plasma near the substrate has revealed how its electron energy evolves as a function of time—increasing gradually during the main pulse and then falling during the positive kick pulse. A transit

time on the order of 1–2 $\mu$s was measured for commuting the plasma potential a distance of ∼15 cm, from the magnetron to the substrate. These measurements are supported by calculations showing that the plasma potential is carried at the electron transport speed. The EEDF follows more closely a Druyvesteyn energy distribution (which has fewer high energy electrons) as opposed to a Maxwellian distribution, but as time goes one even more high energy electrons are removed. The EEDF is predicted well by a Boltzmann equation solver using a value of 0.2 Td. The plasma at the substrate is observed to increase in density immediately after the end of the magnetron pulse and then decay more slowly when using a positive voltage reversal on the target as compared to not using one on the target. An implication of this phenomena is that it may allow one to develop methods that can combine etching and deposition to form smooth uniform films on rough surfaces, since the ion energy hitting the substrate can be controlled by the magnitude of the positive pulse voltage and a relatively dense plasma can be maintained near the substrate. Future applications of this method will be used to measure EEDFs during deposition processes and correlate them to the resultant film properties.

## Acknowledgments

The work in this publication was funded by the Department of Energy Award DE-SC0020689. This research was done with the assistance of the staff and students at Starfire Industries and the Center of Plasma Material Interactions at the University of Illinois at Urbana-Champaign.

## Data availability statement

All data that support the findings of this study are included within the article (and any supplementary files).

## ORCID iDs

David Barlaz https://orcid.org/0000-0001-8915-2059
David N Ruzic https://orcid.org/0000-0001-9501-1439

## References

[1] Keraudy J, Viloan R P B, Raadu M A, Brenning N, Lundin D and Helmersson U 2019 *Surf. Coat. Technol.* **359** 433–7
[2] Viloan R P B, Helmersson U and Lundin D 2021 *Surf. Coat. Technol.* **422** 127487
[3] Avino F, Fonnesu D, Koettig T, Bonura M, Senatore C, Perez Fontenla A T, Sublet A and Taborelli M 2020 *Thin Solid Films* **706** 138058
[4] Houlahan T J, Haehnlein I, Huber W M, Jurczyk B E, Shchelkanov I A and Stubbers R A 2021 High-quality, conformal bellows coatings using ultra-fast HiPIMS with precision ion energy control *Proc. 12th Int. Particle Accelerator Conf. (IPAC'21)* (Campinas, Brazil) pp 3626–9
[5] Ruzic D N, Stubbers R A and Jurczyk B E 2021 *Pulsed Power Module with Pulse an Ion* 11,069,515 B2
[6] Wu B, Haehnlein I, Shchelkanov I, McLain J, Patel D, Uhlig J, Jurczyk B, Leng Y and Ruzic D N 2018 *Vacuum* **150** 216–21
[7] McLain J, Raman P, Patel D, Spreadbury R, Uhlig J, Shchelkanov I and Ruzic D N 2018 *Vacuum* **155** 559–65
[8] Meng L, Cloud A N, Jung S and Ruzic D N 2011 *J. Vac. Sci. Technol.* A **29** 011024
[9] Gudmundsson J T, Alami J and Helmersson U 2002 *Surf. Coat. Technol.* **161** 249–56
[10] Drache S, Stranak V, Herrendorf A-P, Cada M, Hubicka Z, Tichy M and Hippler R 2013 *Vacuum* **90** 176–81
[11] Vetushka A and Ehiasarian A P 2008 *J. Phys. D: Appl. Phys.* **41** 015204
[12] Hippler R, Hubicka Z, Cada M, Ksirova P, Wulff H, Helm C A and Stranak V 2017 *J. Appl. Phys.* **121** 171906
[13] Gudmundsson J T, Sigurjonsson P, Larsson P, Lundin D and Helmersson U 2009 *J. Appl. Phys.* **105** 123302
[14] Gudmundsson J T, Alami J and Helmersson U 2001 *Appl. Phys. Lett.* **78** 3427–9
[15] Pajdarová A D, Kozák T, Hubička Z, Čada M, Mareš P and Čapek J 2020 *Plasma Sources Sci. Technol.* **29** 085016
[16] Hippler R, Cada M and Hubicka Z 2020 *Appl. Phys. Lett.* **116** 064101
[17] Zhou G, Wang L, Wang X and Yu Y 2020 *Vacuum* **175** 109253
[18] Wilson J L, Caughman J B O, Nguyen P L and Ruzic D N 1989 *J. Vac. Sci. Technol.* A **7** 972–6
[19] Caughman J B O, Ruzic D N, Hoffman D J, Langley R A and Lewis M B 1990 *J. Vac. Sci. Technol.* A **8** 4011–6
[20] Ruzic D N 1994 *Electric Probes for Low Temperature Plasmas* (New York: American Vacuum Society)
[21] Lieberman M and Lichtenberg A 2005 *Principles of Plasma Discharges and Materials Processing* 2nd edn (New York: Wiley)
[22] Turkot R B and Ruzic D N 1993 *J. Appl. Phys.* **73** 2173–9
[23] Pahl A 2014 Electron energy distribution function (COMSOL Blog)
[24] Gudmundsson J T, Brenning N, Lundin D and Helmersson U 2012 *J. Vac. Sci. Technol.* A **30** 030801
[25] Stranak V, Herrendorf A P, Drache S, Cada M, Hubicka Z, Bogdanowicz R, Tichy M and Hippler R 2012 *J. Appl. Phys.* **112** 093305
[26] Tan W P S 1973 *J. Appl. Phys.* **44** 3550–6
[27] Seo S-H and Chang H-Y 2004 *Phys. Plasmas* **11** 3595–601
[28] Zhang Y, He X, Chen J, Lu J, Ni X and Shen Z 2015 *3rd Int. Symp. Laser Interact. with Matter* vol 9543 p 95430Z
[29] Mayorov S A 2013 *Bull. Lebedev Phys. Inst.* **40** 258–64
[30] Ivanov I, Statev S, Orlinov V and Shkevov R 1992 *Vacuum* **43** 837–42
[31] Pajdarová A D, Vlček J, Kudláček P and Lukáš J 2009 *Plasma Sources Sci. Technol.* **18** 025008
[32] Hagelaar G J M and Pitchford L C 2005 *Plasma Sources Sci. Technol.* **14** 722–33
[33] Biagi S F 2021 Personal communication: cross sections extracted from PROGRAM MAGBOLTZ *(version 7.1)* www.lxcat.net
[34] Pitchford L C *et al* 2017 *Plasma Process. Polym.* **14** 1600098
[35] Jeckell Z, Barlaz D E, Houlahan T, Hube W, Haehnlein I, Jurczyk B and Ruzic D N 2022 *Plasma Sources, Sci. Technol.* submitted
[36] Mora P 2003 *Phys. Rev. Lett.* **90** 185002